J|A|C|S
ARTICLES

Published on Web 12/21/2010

Dissection of Complex Molecular Recognition Interfaces

Christopher A. Hunter,* Maria Cristina Misuraca, and Simon M. Turega

Department of Chemistry, University of Sheffield, Sheffield S3 7HF, United Kingdom

Received September 20, 2010; E-mail: c.hunter@sheffield.ac.uk

Abstract: The synthesis of a family of zinc porphyrins and pyridine ligands equipped with peripheral H-bonding functionality has provided access to a wide range of closely related supramolecular complexes featuring between zero and four intramolecular H-bonds. An automated UV/vis titration system was used to characterize 120 different complexes, and these data were used to construct a large of number of different chemical double mutant cycles to quantify the intramolecular H-bonding interactions. The results probe the quantitative structure−activity relationship that governs cooperativity in the assembly of complex molecular recognition interfaces. Specifically, variations in the chemical structures of the complexes have allowed us to change the supramolecular architecture, conformational flexibility, geometric complementarity, the number and nature of the H-bond interactions, and the overall stability of the complex. The free energy contributions from individual H-bonds are additive, and there is remarkably little variation with architecture in the effective molarity for the formation of intramolecular interactions. Intramolecular H-bonds are not observed in complexes where they are geometrically impossible, but there are no cases where excellent geometric complementarity leads to very high affinities. Similarly, changes in conformational flexibility seem to have limited impact on the values of effective molarity (*EM*). The major variation that was found for all of the 48 intramolecular interactions that were examined using double mutant cycles is that the values of *EM* for intramolecular carboxylate ester−phenol H-bonds (200 mM) are an order of magnitude larger than those found for phosphonate diester−phenol H-bonds (30 mM). The corresponding intermolecular phosphonate diester−phenol H-bonds are 2 orders of magnitude more stable than carboxylate ester−phenol H-bonds, and the large differences in *EM* may be due to some kind of compensation effect, where the stronger H-bond is harder to make, because it imposes tighter constraints on the geometry of the complex.

Introduction

Self-assembly and self-organization in biological systems are characterized by complex recognition interfaces between macromolecular surfaces with multiple cooperative intermolecular interactions.[1] Many different factors are recognized to contribute to the thermodynamic properties of these interfaces: electrostatic interactions between charges, H-bonds, aromatic interactions, desolvation, etc. This complexity makes it difficult to disentangle the relative contributions of individual interaction sites and the cooperativity involved in assembly of the entire interface.[2] The inherent conformational flexibility of biomolecules and the changes in conformational dynamics that are associated with complex formation add to the problem.[3] Synthetic supramolecular systems provide a controlled environment, where some of these variables can be systematically studied. This has provided insight into the magnitude of specific functional group contacts, the requirements for filling space, the role of desolvation, and cooperativity between multiple interactions.[4] For synthetic supramolecular systems that use strong binding site interactions and relatively rigid molecular frameworks, cooperativity is usually observed as additive free energy contributions from the individual interaction sites.[5] However, the behavior of systems that feature multiple weak interactions between flexible molecules, such as biomolecules, is more complicated.

(1) (a) Mulder, A.; Huskens, J.; Reinhoudt, D. N. *Org. Biomol. Chem.* **2004**, *2*, 3409. (b) Philp, D.; Stoddart, J. F. *Angew. Chem., Int. Ed. Engl.* **1996**, *35*, 1155. (c) Lehn, J. M. *Angew. Chem., Int. Ed. Engl.* **1990**, *29*, 1304. (d) Badjic, J. D.; Nelson, A.; Cantrill, S. J.; Turnbull, W. B.; Stoddart, J. F. *Acc. Chem. Res.* **2005**, *38*, 723. (e) Mammen, M.; Choi, S. K.; Whitesides, G. M. *Angew. Chem., Int. Ed.* **1998**, *37*, 2755. (f) Kay, E. R.; Leigh, D. A.; Zerbetto, F. *Angew. Chem., Int. Ed.* **2007**, *46*, 72. (g) Kolomiets, E.; Lehn, J. M. *Chem. Commun.* **2005**, 1519. (h) Hoffmann, M.; Karnbratt, J.; Chang, M. H.; Herz, L. M.; Albinsson, B.; Anderson, H. L. *Angew. Chem., Int. Ed.* **2008**, *47*, 4993.

(2) (a) Williams, D. H.; Bardsley, B. *Angew. Chem., Int. Ed.* **1999**, *38*, 1173. (b) Williams, D. H.; Stephens, E.; O'Brien, D. P.; Zhou, M. *Angew. Chem., Int. Ed.* **2004**, *43*, 6596. (c) Baldini, L.; Ballester, P.; Casnati, A.; Gomila, R. M.; Hunter, C. A.; Sansone, F.; Ungaro, R. *J. Am. Chem. Soc.* **2003**, *125*, 14181. (d) Hughes, A. D.; Anslyn, E. V. *Proc. Natl. Acad. Sci. U.S.A.* **2007**, *104*, 6538. (e) Tobey, S. L.; Anslyn, E. V. *J. Am. Chem. Soc.* **2003**, *125*, 10963. (f) Camara-Campos, A.; Hunter, C. A.; Tomas, S. *Proc. Natl. Acad. Sci. U.S.A.* **2006**, *103*, 3034. (g) Lemonnier, J. F.; Guenee, L.; Bernardinelli, G.; Vigier, J. F.; Bocquet, B.; Piguet, C. *Inorg. Chem.* **2010**, *49*, 1252–1265. (h) Calderone, C. T.; Williams, D. H. *J. Am. Chem. Soc.* **2001**, *123*, 6262. (i) Shiozawa, H.; Chia, B. C. S.; Davies, N. L.; Zerella, R.; Williams, D. H. *J. Am. Chem. Soc.* **2002**, *124*, 3914. (j) Williams, D. H.; Davies, N. L.; Zerella, R.; Bardsley, B. *J. Am. Chem. Soc.* **2004**, *126*, 2042.

(3) (a) Wang, T. J.; Hoy, J. A.; Lamm, M. H.; Nilsen-Hamilton, M. *J. Am. Chem. Soc.* **2009**, *131*, 14747. (b) Menand, M.; Jabin, I. *Chem.* **2010**, *16*, 2159. (c) Koshland, D. E. *Proc. Natl. Acad. Sci. U.S.A.* **1958**, *44*, 98. (d) Anderson, H. L.; Hunter, C. A.; Meah, M. N.; Sanders, J. K. M. *J. Am. Chem. Soc.* **1990**, *112*, 5780.

(4) (a) Cockroft, S. L.; Hunter, C. A. *Chem. Commun.* **2006**, 3806. (b) Cockroft, S. L.; Hunter, C. A. *Chem Commun.* **2009**, 3961. (c) Fischer, F. R.; Schweizer, W. B.; Diederich, F. *Chem. Commun.* **2008**, 4031. (d) Hof, F.; Scofield, D. M.; Schweizer, W. B.; Diederich, F. *Angew. Chem., Int. Ed.* **2004**, *43*, 5056. (e) Scarso, A.; Trembleau, L.; Rebek, J. *J. Am. Chem. Soc.* **2004**, *126*, 13512.

10.1021/ja1084783

Practical experience in the fields of both medicinal and supramolecular chemistry shows that preorganization of the binding partners improves affinity. The dogma is that conformational restriction of the molecules reduces the entropic cost of freezing rotors, so that rigid molecules are preferred. However, in practice, it is very difficult to experimentally separate this kind of entropic contribution from the observed free energy of binding, because the entropy change is a property of the system as a whole. Thus, the enthalpy and entropy of binding often show large fluctuations that are not expressed in a change in affinity. Changes in the structure of the solvent or a macromolecule can lead to very large changes in enthalpy and entropy that more or less cancel out, and these effects swamp the small differences that could be caused by conformational restriction. Moreover, the introduction of conformational restriction into a compound changes more than the number of torsional degrees of freedom: first, a conformational lock can fix the compound in a geometry that would otherwise be inaccessible without a significant energy penalty, that is, enthalpic strain; second, a conformational lock will prevent the compound from interacting with alternative sites in an undesired binding mode; and, third, the conformational lock will usually involve addition of functional groups that may make direct contacts with the binding site. Thus, there are many mechanisms by which the restriction of conformational mobility may improve binding affinity without the need to invoke an entropic contribution due to restriction of rotors. Here, we describe a supramolecular model system that we can use as a controlled environment for dissecting thermodynamic contributions to a cooperative recognition interface that involves multiple weak interactions between flexible molecules.

Approach

There are two parameters that quantify cooperativity in a system that makes multiple noncovalent interactions: the allosteric interaction parameter, which measures the change in intrinsic functional group interaction energy; and the effective molarity, *EM*, which measures the extent to which intramolecularity enhances the probability of making a functional group interaction (Figure 1).[6] The factors that contribute to the intrinsic functional group interaction energy are reasonably well-understood: steric hindrance, secondary electrostatic interactions, functional group polarization, etc. The relationship between supramolecular architecture and *EM* is less obvious. One might expect that *EM* will decrease with conformational strain in the bound state and restriction of conformational flexibility, but the magnitude of these effects is difficult to predict. We have therefore designed a set of receptors and ligands with varying degrees of complementarity and conformational flexibility in an attempt to map this relationship.

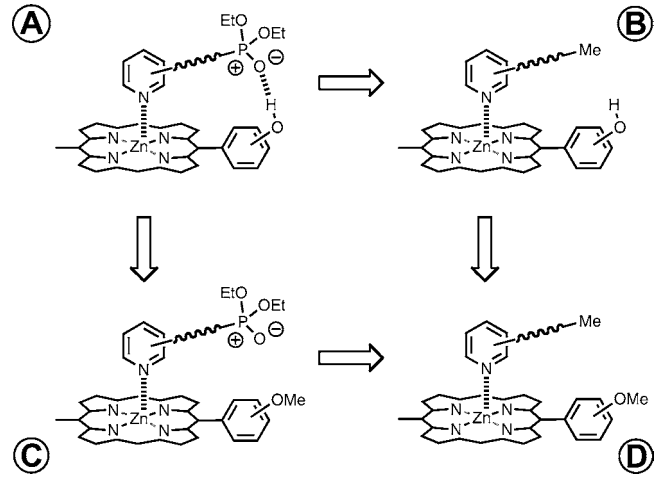

Figure 1. A chemical double mutant cycle designed to measure the free energy contribution of the intramolecular H-bond in complex A to the overall stability of the complex ($\Delta\Delta G^\circ$ in eq 1).

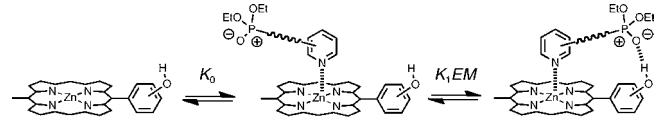

Figure 2. Stepwise equilibria in the formation of complex A in Figure 1. K_0 is the intermolecular association constant for formation of the zinc−nitrogen interaction. K_1EM is the intramolecular equilibrium constant for formation of the H-bond.

We have shown previously that a strong zinc porphyrin−pyridine coordination bond can be used to facilitate cooperative formation of a weaker intramolecular H-bond. By using reference compounds (mutants) where one of the interaction sites has been deleted, it is possible to construct a chemical double mutant cycle (DMC) to quantify the contribution that the intramolecular H-bond makes to the overall stability of complex A in Figure 1 using eq 1.[7]

$$\Delta\Delta G^\circ = \Delta G^\circ_{\mathrm{A}} - \Delta G^\circ_{\mathrm{B}} - \Delta G^\circ_{\mathrm{C}} + \Delta G^\circ_{\mathrm{D}} \qquad (1)$$

The DMC removes all allosteric effects (secondary interactions, changes in zinc−nitrogen interaction, etc.), so that the thermodynamic contribution of the H-bond between two functional groups can be dissected from all of the other factors that affect the overall stability of complex A. If we consider the assembly of complex A as a stepwise process, where an intermolecular coordination bond is formed first, followed by an intramolecular H-bond, then the cooperativity in the assembly of this complex can be quantified by the effective molarity for the intramolecular process (*EM* in Figure 2). Thus, the free energy contribution of the intramolecular H-bond to the overall stability of complex A is given by eq 2.

$$\Delta\Delta G^\circ = -RT\ln(K_1EM) \qquad (2)$$

where K_1 is the corresponding intermolecular association constant for formation of the same H-bond between two appropriate reference compounds, where no other interactions are possible.

(5) (a) Drobizhev, M.; Stepanenko, Y.; Rebane, A.; Wilson, C. J.; Screen, T. E. O.; Anderson, H. L. *J. Am. Chem. Soc.* **2006**, *128*, 12432. (b) Camara-Campos, A.; Hunter, C. A.; Tomas, S. *Proc. Natl. Acad. Sci. U.S.A.* **2006**, *103*, 3034. (c) Hunter, C. A.; Ihekwaba, N.; Misuraca, M. C.; Segarra-Maset, M. D.; Turega, S. M. *Chem. Commun.* **2009**, 3964.

(6) (a) Fersht, A. R.; Kirby, A. J. *J. Am. Chem. Soc.* **1967**, *89*, 4857. (b) Benedetti, F.; Stirling, C. J. M. *Chem. Commun.* **1983**, 1374. (c) Sinclair, A. J.; del Amo, V.; Philp, D. *Org. Biomol. Chem.* **2009**, *7*, 3308. (d) Chi, X. L.; Guerin, A. J.; Haycock, R. A.; Hunter, C. A.; Sarson, L. D. *Chem. Commun.* **1995**, 2563. (e) Hunter, C. A.; Tomas, S. *Chem. Biol.* **2003**, *10*, 1023. (f) Cacciapaglia, R.; Di Stefano, S.; Mandolini, L. *Acc. Chem. Res.* **2004**, *37*, 113. (g) Kirby, A. *Adv. Phys. Org. Chem.* **1980**, *17*, 183. (h) Hunter, C. A.; Anderson, H. L. *Angew. Chem., Int. Ed.* **2009**, *48*, 7488.

(7) (a) Cockroft, S. L.; Hunter, C. A. *Chem. Soc. Rev.* **2007**, *36*, 172. (b) Camara-Campos, A.; Musumeci, D.; Hunter, C. A.; Turega, S. *J. Am. Chem. Soc.* **2009**, *131*, 18518.

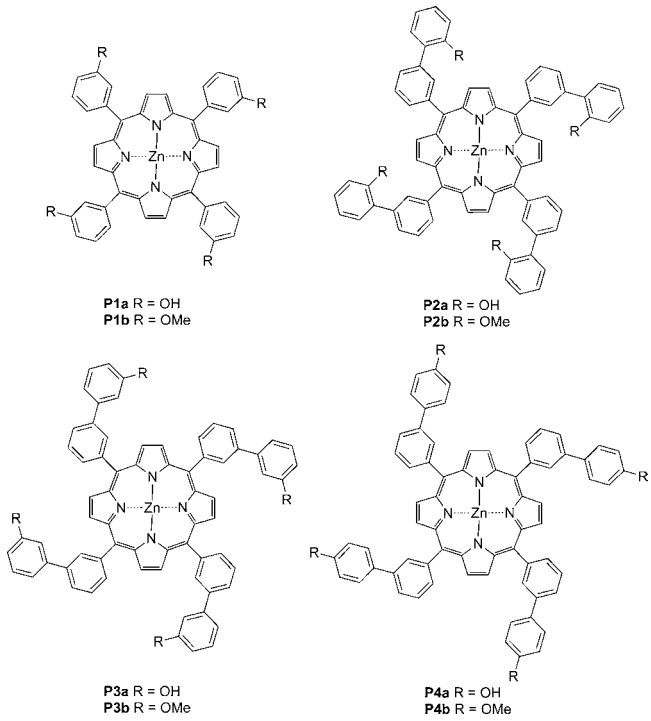

Figure 3. Porphyrin receptors, **P1a**−**P4a** (R = OH) and **P1b**−**P4b** (R = OMe).

If the association constant for the intermolecular H-bond, K_1, can be measured using reference compounds, then the DMC can be used to determine the value of *EM* for the intramolecular interaction in complex A using eq 2. The system illustrated in Figure 1 therefore provides an ideal platform for exploring the relationship between the structures of the groups linking the two interaction sites on both the porphyrin receptor and the ligand and the magnitude of the *EM*.[8] The use of a phenol as the H-bond donor ($\alpha = 3.8$) and a phosphonate diester as the H-bond acceptor ($\beta = 8.9$) ensures that the H-bond interaction is sufficiently strong to allow measurement of K_1 in nonpolar solvents.[9] Figures 3 and 4 illustrate a range of readily accessible metalloporphyrins and ligands that can be combined in a combinatorial manner to construct a large number of DMCs for different supramolecular architectures and thereby begin to characterize the relationship between chemical structure and *EM*.

Results and Discussion

Porphyrin Receptor Synthesis. Free base porphyrins **1** and **2** were prepared according to literature procedures.[10] Metalation with zinc acetate provided receptors **P1a** and **P1b** (Scheme 1). Two different routes were investigated for the synthesis of the other receptor architectures. In route I (Scheme 2), Suzuki couplings between tetrabromoporphyrin **3** and 2-, 3-, or 4-hydroxyphenylboronic acid only proceeded in good yield for the 3-isomer, **4**. The 2- and 4-isomers, **5** and **6**, can be obtained by route I, but in very low yield. The alternative route (II) shown in Scheme 3 proved to be superior. Suzuki coupling of 3-bromobenzaldehyde with 2-, 3-, or 4-methoxyphenylboronic

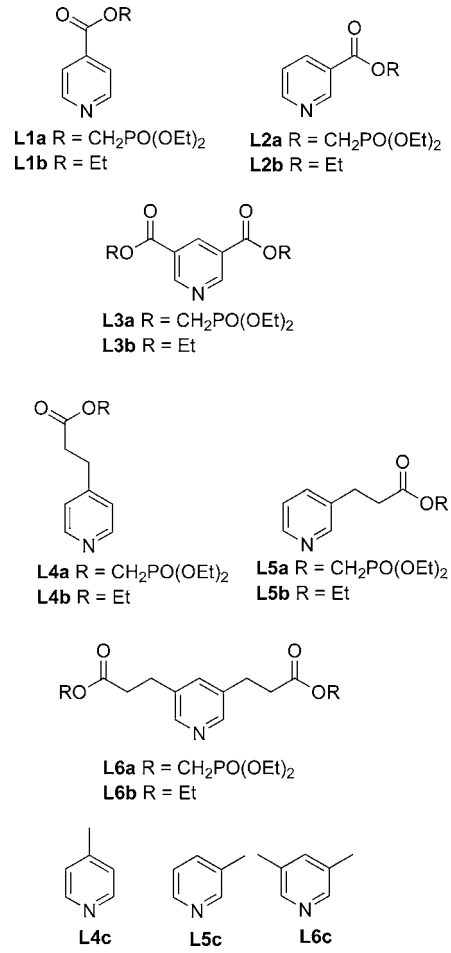

Figure 4. Ligand structures, **L1a**−**L6a** (R = $CH_2PO(OEt)_2$), **L1b**−**L6b** (R = Et), and **L4c**−**L6c**.

Scheme 1. Synthesis of Zinc Porphyrin Receptors **P1a** and **P1b**

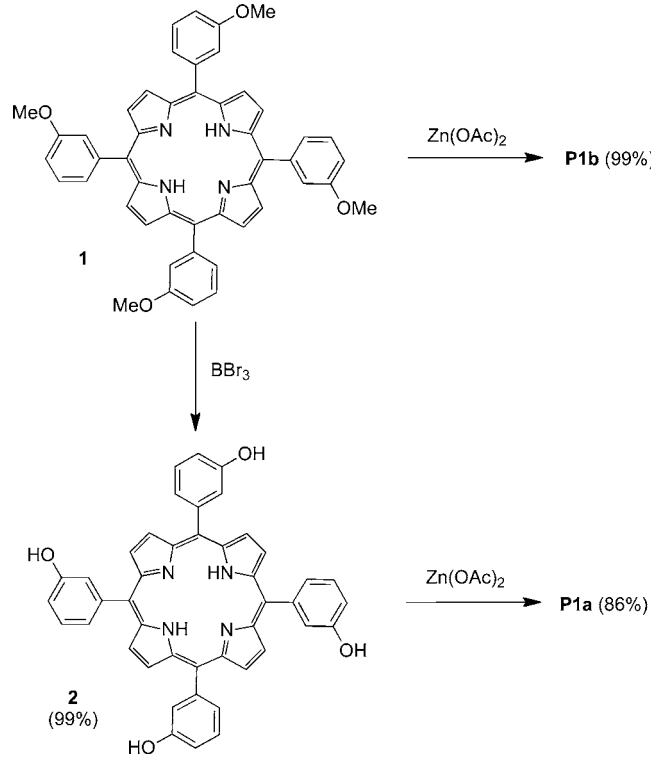

(8) Chekmeneva, E.; Hunter, C. A.; Packer, M. J.; Turega, S. M. *J. Am. Chem. Soc.* **2008**, *130*, 17718.
(9) (a) Abraham, M. H.; Platts, J. A. *J. Org. Chem.* **2001**, *66*, 3484. (b) Hunter, C. A. *Angew. Chem., Int. Ed.* **2004**, *43*, 5310.

Scheme 2. Route I for Synthesis of the Zinc Porphyrin Receptors

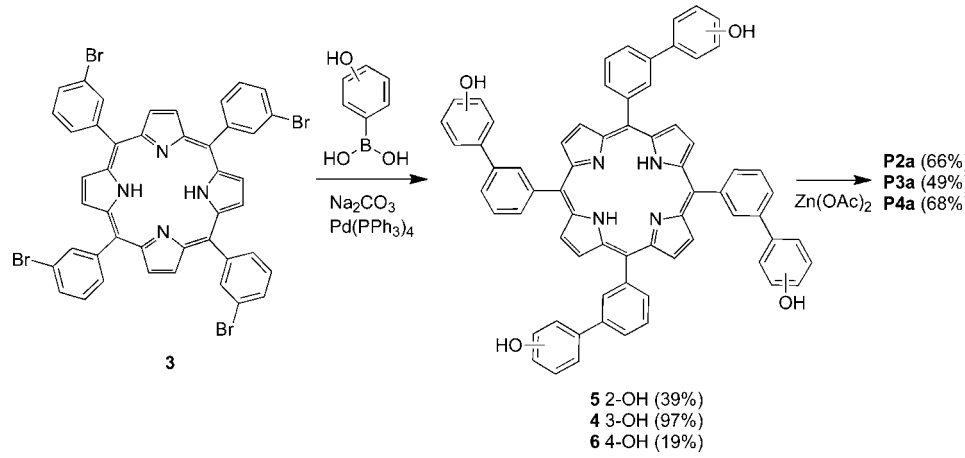

Scheme 3. Route II for Synthesis of the Zinc Porphyrin Receptors

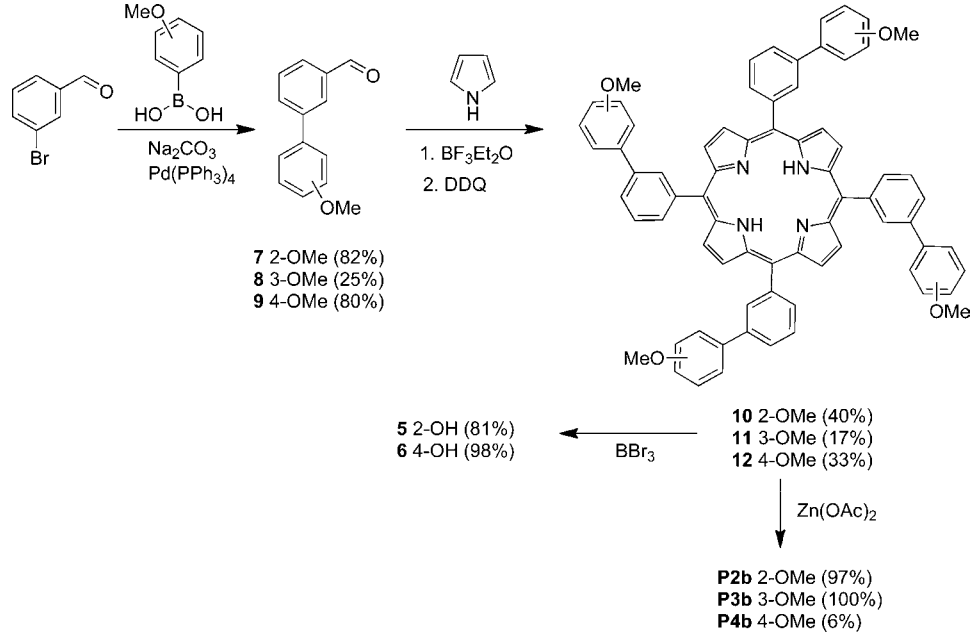

acid gave the corresponding biphenyl aldehydes **7**, **8**,[10] and **9**. The aldehydes were converted to the corresponding free-base porphyrins **10**, **11**, and **12** using the Lindsey method.[11] The tetramethoxyporphyrins **10** and **11** were deprotected with BBr_3 to give the corresponding tetrahydroxyporphyrins (Scheme 3). Metalation of the free base porphyrins with zinc acetate gave the corresponding porphyrin receptors **P2a**, **P3a**, **P4a** (Scheme 2), **P2b**, **P3b**, and **P4b** (Scheme 3).

Ligand Synthesis. Some of the ligands, ethyl nicotinate, ethyl isonicotinate, 3-picoline, 4-picoline, and 3,5-lutidine (corresponding to **L2b**, **L1b**, **L4c**, **L5c**, and **L6c**, respectively), were commercially available. Ligands **L2a**, **L3a**, and **L3b** were synthesized according to previously published procedures.[8] The remaining ligands were synthesized from the corresponding carboxylic acids. The dicarboxylic acid, **15**, is the only acid that is not commercially available, and this was prepared using the route shown in Scheme 4. Sonogashira coupling of propargyl alcohol with 3,5-dibromopyridine gave diol **13**, which was reduced using a Pd/C CatCart in a H-cube apparatus to provide **14**.[12] Diol **14** was oxidized to the corresponding diacid with Jones reagent, but this compound proved easier to isolate as the diethyl ester after refluxing with acidic ethanol. The diester, which corresponds to one of the control ligands, **L6b**, was then hydrolyzed to give the diacid **15**. Carboxylic acids **16** and **17** were coupled with diethyl hydroxymethane phosphonate using *N*,*N*′-dicyclohexylcarbodiimide (DCC) and 4-dimethylaminopyridine (DMAP) to yield ligands **L1a** and **L5a**. To convert carboxylic acids **18** and **15** into ligands **L4a** and **L6a**, diethyl hydroxymethane phosphonate was first tosylated to give **19**,[13]

(10) (a) Crossley, M. J.; Field, L. D.; Forster, A. J.; Harding, M. M.; Sternhell, S. *J. Am. Chem. Soc.* **1987**, *109*, 341. (b) Wiehe, A.; Shaker, Y. M.; Brandt, J. C.; Mebs, S.; Senge, M. O. *Tetrahedron* **2005**, *61*, 5535.

(11) Lindsey, J. S.; Schreiman, I. C.; Hsu, H. C.; Kearney, P. C.; Marguerettaz, A. M. *J. Org. Chem.* **1987**, *52*, 827.

(12) Mor, M.; Rivara, S.; Lodola, A.; Plazzi, P. V.; Tarzia, G.; Duranti, A.; Tontini, A.; Piersanti, G.; Kathuria, S.; Piomelli, D. *J. Med. Chem.* **2004**, *47*, 4998.

(13) (a) Desai, B.; Kappe, C. O. *J. Comb. Chem.* **2005**, *7*, 641. (b) Saaby, S.; Knudsen, K. R.; Ladlow, M.; Ley, S. V. *Chem. Commun.* **2005**, 2909. (c) Thales Nanotechnology Inc. website: http://www.thalesnano.com.

Scheme 4. Synthesis of Dicarboxylic Acid **15**

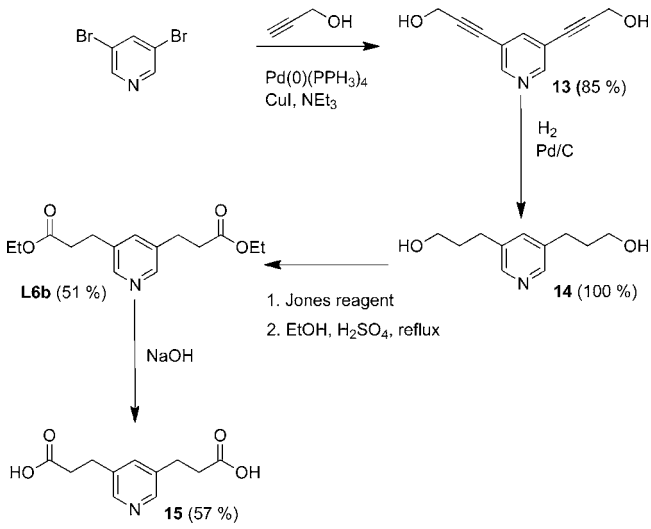

Scheme 5. Synthesis of Ligands

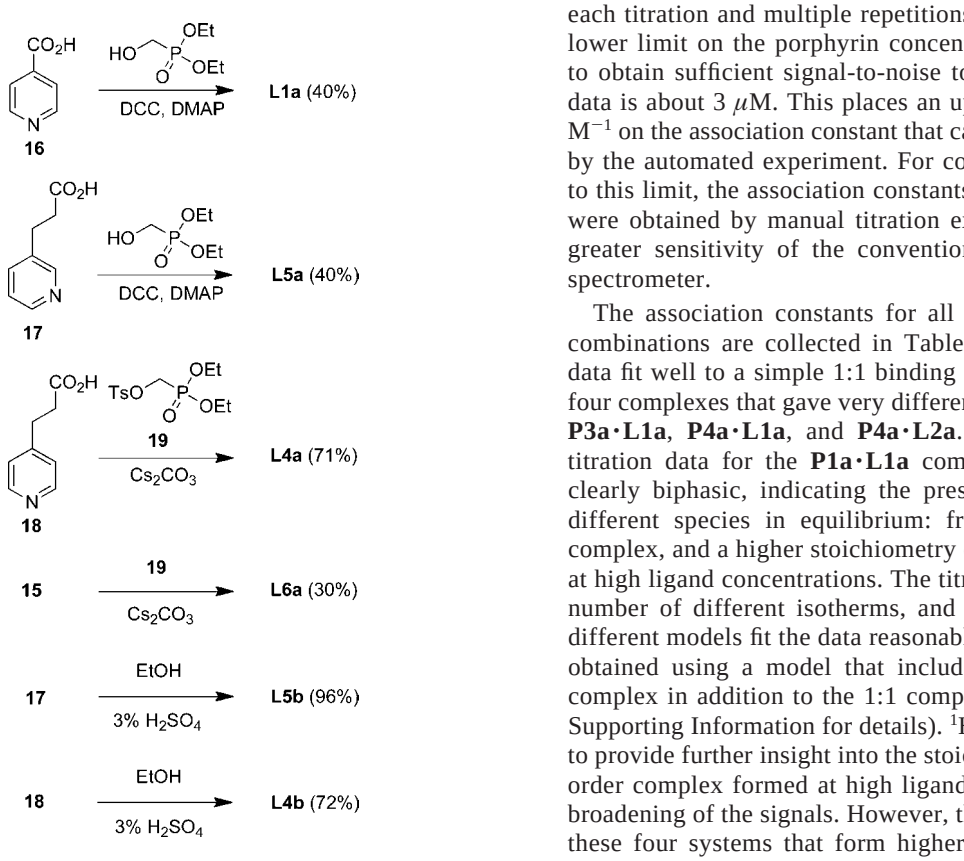

which underwent nucleophilic substitution under basic conditions to give the esters in high yield. Carboxylic acids **17** and **18** were esterified in acidic EtOH to give control ligands **L5b** and **L4b** (Scheme 5).

High Throughput Titration Analysis of Binding. Interaction of the ligands with the porphyrin receptors was analyzed using UV/vis titration experiments. Complexation of the pyridine nitrogen of a ligand to the zinc center of a porphyrin causes a change of approximately 10 nm in the UV/vis absorption maximum of the Soret band (Figure 5a), and this change was used to determine association constants. However, the large number of porphyrin−ligand combinations encouraged us to develop an automated approach to collection of the spectroscopic data. A UV/vis plate reader equipped with internal syringes was programmed to titrate ligand into receptor with acquisition of the UV/vis spectrum after each addition. A potential disadvantage of this system is that the plate is open to the atmosphere, but the use of a nonpolar high boiling point solvent, toluene, minimizes potential problems due to solvent evaporation and absorption of atmospheric water. The association constants obtained using the plate reader agree very well with those obtained from conventional manual titrations: representative titration data for automated and manual experiments on the **P1a·L1b** complex are shown in Figure 5b and c, respectively. There is a well-defined isosbestic point (Figure 5a), and the titration data fit well to a 1:1 isotherm (Figure 5b and c). The association constants for automated and manual experiments are identical within experimental error: the average value over three different experiments is 2600 ± 500 M^{-1} for the automated experiment and 2200 ± 100 M^{-1} for the manual titration. The errors tend to be somewhat higher for automated experiments, but this is balanced against the speed advantage, which allows collection of a large number of data points for each titration and multiple repetitions of each titration. The lower limit on the porphyrin concentration that is required to obtain sufficient signal-to-noise to ensure good titration data is about 3 μM. This places an upper limit of about 10^7 M^{-1} on the association constant that can be reliably measured by the automated experiment. For complexes that are close to this limit, the association constants that are reported here were obtained by manual titration experiments, due to the greater sensitivity of the conventional UV/vis absorption spectrometer.

The association constants for all 120 porphyrin−ligand combinations are collected in Table 1. In most cases, the data fit well to a simple 1:1 binding isotherm, but there are four complexes that gave very different isotherms: **P1a·L1a**, **P3a·L1a**, **P4a·L1a**, and **P4a·L2a**. Figure 5e shows the titration data for the **P1a·L1a** complex. The isotherm is clearly biphasic, indicating the presence of at least three different species in equilibrium: free porphyrin, the 1:1 complex, and a higher stoichiometry complex that is formed at high ligand concentrations. The titration data were fit to a number of different isotherms, and although a number of different models fit the data reasonably well, the best fit was obtained using a model that includes formation of a 2:5 complex in addition to the 1:1 complex (Figure 5e, see the Supporting Information for details). ^{1}H NMR titrations failed to provide further insight into the stoichiometry of the higher order complex formed at high ligand concentrations due to broadening of the signals. However, the reason that it is only these four systems that form higher order complexes will become clear based on the DMC analysis in the next section of this Article. In short, all four of the complexes that exhibit this anomalous behavior are systems where intramolecular phosphonate−phenol H-bonds are difficult to make. Thus, the only way in which the H-bonding potential of these groups can be satisfied is through intermolecular interactions between two porphyrin complexes. Dimerization of the porphyrin complexes establishes a template for binding multiple bridging ligands via pyridine−phenol and phosphonate−phenol H-bonds (Figure 6). For ligands that have only one phosphonate group, the 2:5 complex is the lowest stoichiometry complex that satisfies the principle of maximum site occupancy, where all of the H-bond and

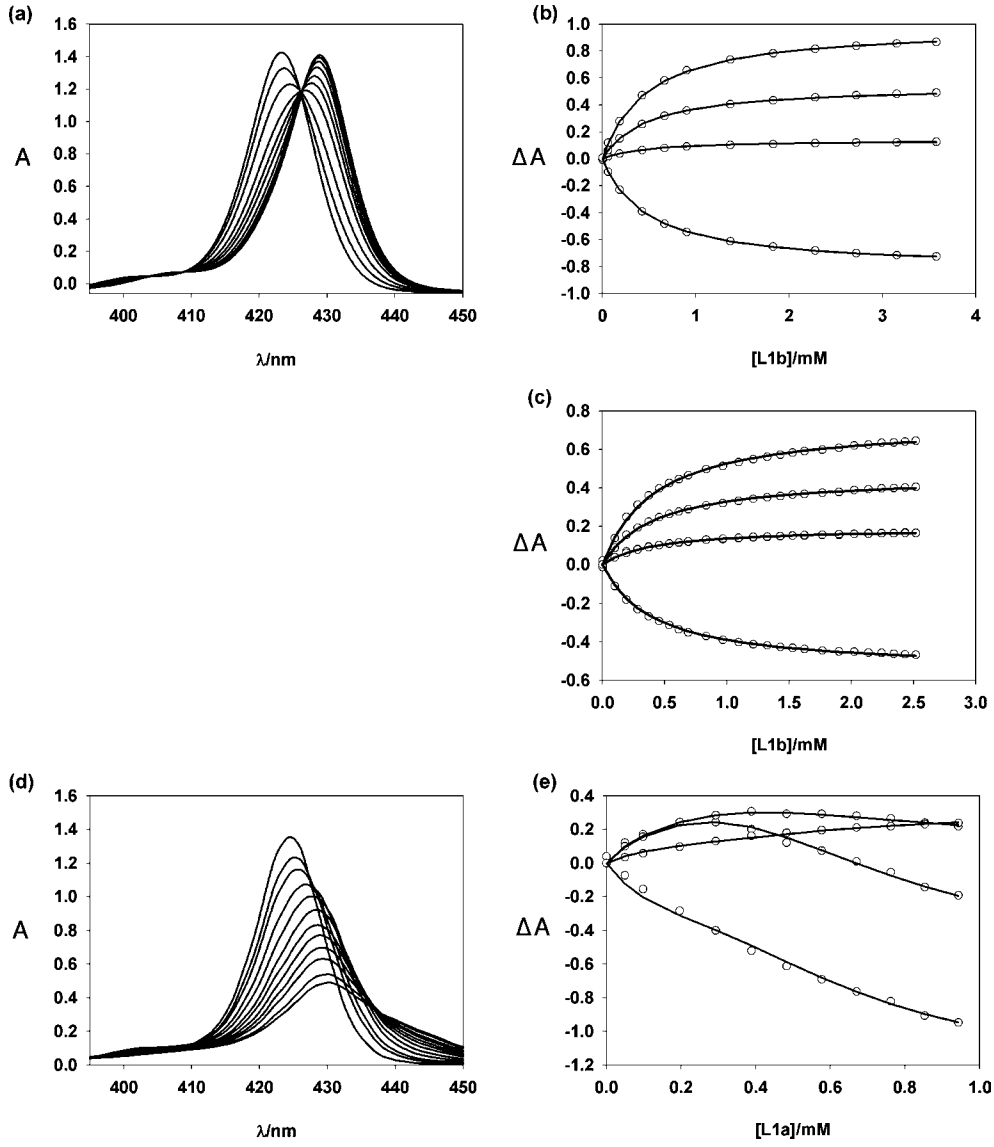

Figure 5. UV/vis titration data in toluene at 298 K. (a) Data for manual titration of **P1a** with **L1b** and (b) the corresponding fit of the absorbance at 420, 425, 430, and 440 nm to a 1:1 binding isotherm. (c) Data for automated titration of **P1a** with **L1b** showing the fit of the absorbance at 420, 425, 430, and 440 nm to a 1:1 binding isotherm. (d) Data for manual titration of **P1a** with **L1a** and (e) the corresponding fit of the absorbance at 420, 425, 430, and 440 nm to a 1:1 plus 2:5 binding isotherm.

Table 1. Association Constants (M^{-1}) for Formation of 1:1 Complexes in Toluene at 298 K (Percentage Errors in Brackets)[a]

	porphyrin							
ligand	**P1a**	**P2a**	**P3a**	**P4a**	**P1b**	**P2b**	**P3b**	**P4b**
L1a	4.0×10^3 (30%)[b]	1.9×10^4 (10%)	1.5×10^4 (10%)[b]	8.2×10^3 (7%)[b]	2.9×10^3 (7%)	2.0×10^3 (3%)	2.4×10^3 (8%)	2.2×10^3 (1%)
L2a	2.4×10^5 (25%)	2.5×10^4 (8%)	9.5×10^4 (30%)	1.6×10^4 (20%)[b]	9.2×10^3 (1%)	7.4×10^3 (3%)	4.6×10^3 (40%)	3.3×10^3 (6%)
L3a	6.5×10^6 (15%)	7.4×10^4 (1%)	9.1×10^5 (3%)	6.4×10^4 (9%)	7.6×10^3 (1%)	2.3×10^3 (9%)	9.1×10^3 (20%)	5.4×10^3 (4%)
L4a	3.8×10^5 (20%)	2.0×10^5 (1%)	1.4×10^6 (2%)	5.9×10^5 (1%)	1.4×10^4 (1%)	1.2×10^4 (2%)	1.9×10^4 (10%)	1.5×10^4 (1%)
L5a	2.7×10^5 (20%)	2.1×10^5 (20%)	4.8×10^5 (1%)	1.2×10^5 (20%)	5.1×10^3 (4%)	4.1×10^3 (2%)	7.1×10^3 (1%)	5.5×10^3 (4%)
L6a	8.9×10^6 (3%)[c]	8.3×10^6 (20%)	9.3×10^6 (20%)[c]	2.2×10^6 (10%)	6.8×10^3 (10%)	4.4×10^3 (7%)	8.2×10^3 (6%)	7.9×10^3 (3%)
L1b	2.6×10^3 (8%)	3.9×10^3 (5%)	6.3×10^3 (2%)	3.5×10^3 (4%)	3.0×10^3 (10%)	2.8×10^3 (7%)	3.8×10^3 (8%)	3.4×10^3 (6%)
L2b	3.6×10^3 (8%)	5.1×10^3 (2%)	8.5×10^3 (1%)	5.1×10^3 (6%)	3.9×10^3 (20%)	3.3×10^3 (6%)	6.2×10^3 (30%)	5.4×10^3 (4%)
L3b	3.2×10^3 (1%)	4.3×10^3 (5%)	6.9×10^3 (9%)	5.1×10^3 (40%)	3.8×10^3 (20%)	2.6×10^3 (10%)	6.0×10^3 (20%)	4.5×10^3 (20%)
L4b	1.6×10^4 (30%)	1.9×10^4 (20%)	3.8×10^4 (20%)	2.5×10^4 (9%)	1.3×10^4 (8%)	1.1×10^4 (30%)	1.9×10^4 (20%)	1.6×10^4 (30%)
L5b	2.1×10^4 (20%)	2.7×10^4 (4%)	5.1×10^4 (2%)	1.2×10^4 (4%)	7.0×10^3 (30%)	5.0×10^3 (10%)	8.6×10^3 (2%)	8.0×10^3 (10%)
L6b	2.7×10^4 (20%)	4.3×10^4 (8%)	1.2×10^5 (9%)	7.3×10^3 (30%)	4.4×10^3 (2%)	2.7×10^3 (3%)	5.7×10^3 (1%)	4.9×10^3 (20%)
L4c	1.2×10^4 (8%)	1.5×10^4 (5%)	2.6×10^4 (20%)	2.1×10^4 (5%)	1.1×10^4 (20%)	9.1×10^3 (1%)	1.6×10^4 (4%)	1.4×10^4 (7%)
L5c	6.7×10^3 (20%)	8.0×10^3 (4%)	1.7×10^4 (2%)	1.1×10^4 (10%)	7.1×10^3 (6%)	5.4×10^3 (20%)	9.1×10^3 (8%)	6.7×10^3 (6%)
L6c	7.5×10^3 (9%)	1.0×10^4 (3%)	1.7×10^4 (2%)	1.5×10^4 (10%)	9.5×10^3 (1%)	7.0×10^3 (1%)	1.3×10^4 (2%)	8.5×10^3 (20%)

[a] Errors are quoted as twice the standard deviation of the values from multiple repeats of the same titration (3−12 repeats). The errors estimated in this way range from 1% to 40%, with an average value of 10% over the entire data set. We therefore assume that ±10% is the real error in the experiment, and this value is used as the lower limit on the error in K in all subsequent analysis. [b] Fitted to a 1:1 plus 2:5 isotherm. [c] Measured by manual titration.

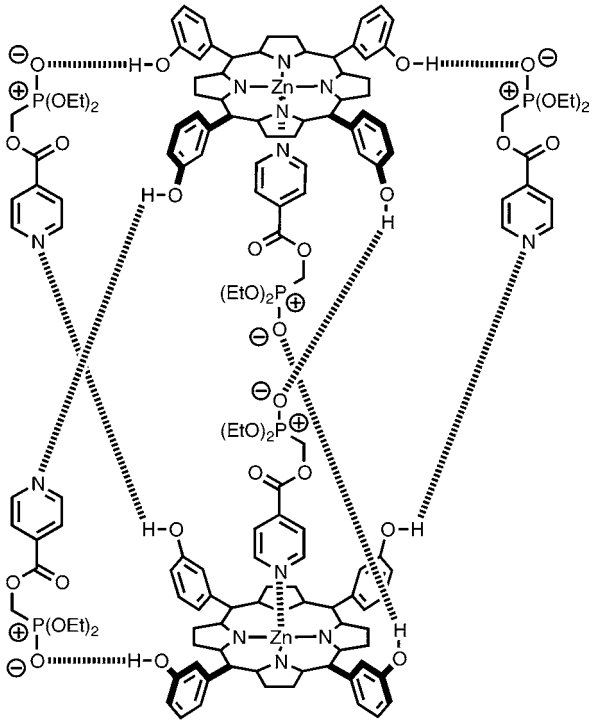

Figure 6. Exploded view of possible intermolecular interactions in the 2:5 complexes formed by ligands that cannot make intramolecular H-bonds in the 1:1 complex (**P1a·L1a**, **P3a·L1a**, **P4a·L1a**, and **P4a·L2a**).

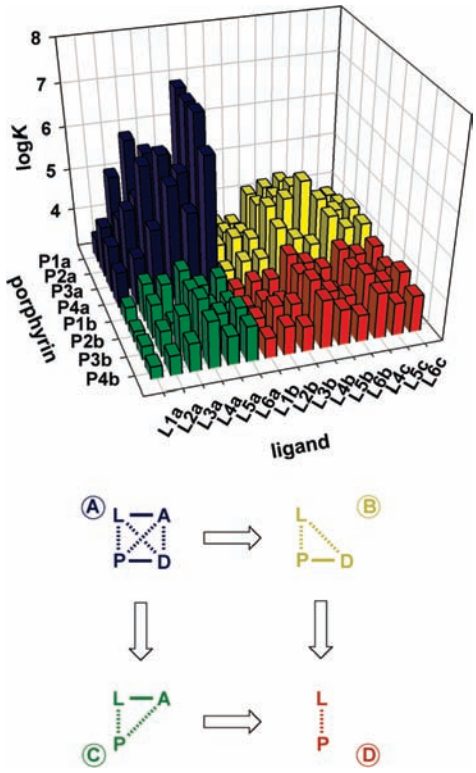

Figure 7. Association constants (log K/M^{-1}) for formation of 1:1 complexes (phosphonate ligand−hydroxyporphyrin complexes in blue, phosphonate ligand−methoxyporphyrin complexes in green, control ligand−hydroxyporphyrin complexes in yellow, and control ligand−methoxyporphyrin complexes in red), and the DMC used to quantify the phosphonate−phenol (A·D) H-bond interaction in porphyrin−ligand (P·L) complexes.

coordination sites on all of the molecules are fully bound. The association constants quoted in Table 1 for these four

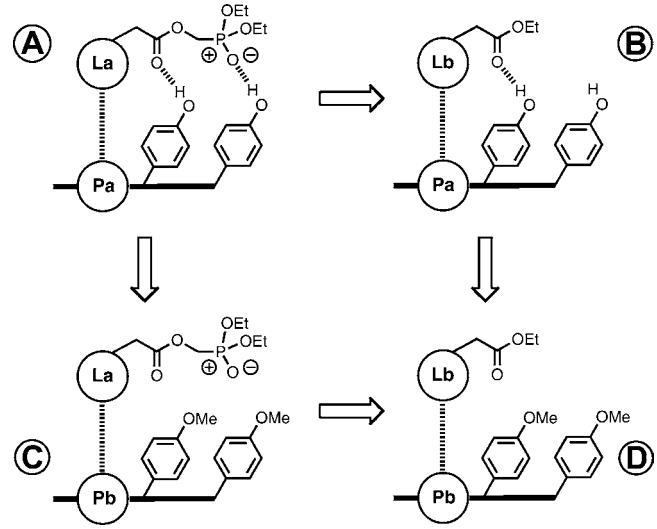

Figure 8. DMC for evaluating the thermodynamic contribution of phosphonate diester−phenol H-bonds to the stability of a porphyrin−ligand complex.

Table 2. Free Energy Contributions from Phosphonate Diester−Phenol H-Bonds ($\Delta\Delta G°$/kJ mol^{-1}) at 298 K in Toluene, Determined Using the Chemical Double Mutant Cycle in Figure 8[a]

	ligand					
porphyrin	**L1a**	**L2a**	**L3a**	**L4a**	**L5a**	**L6a**
P1a	-1	-8	-17	-8	-7	-13
P2a	-5	-2	-7	-6	-6	-12
P3a	-3	-7	-11	-9	-6	-10
P4a	-3	-4	-6	-8	-7	-13

[a] Complexes that make weak H-bonds are shaded (cf., Figure 9). Errors are ±1 kJ mol^{-1}.

systems are the values for the 1:1 complexes that are formed at low ligand concentrations.

Thermodynamics of Phosphonate Diester−Phenol H-Bonding. The results in Table 1 are illustrated graphically in Figure 7. The complexes are grouped into families according to the four components of the DMC. The blue region shows the results for complexes formed between the porphyrins that contain phenol H-bond donors (**P1a**−**P4a**) and the ligands that contain phosphonate H-bond acceptors (**L1a**−**L6a**). In general, these complexes are more stable than the other complexes that do not have the potential to form phosphonate−phenol H-bonds. However, within this family, there is considerable variation in stability due to differences in the number and the geometry of the H-bond interactions. Some of the blue complexes have a stability similar to that of the control complexes, indicating that no intramolecular phosphonate−phenol H-bonds are formed, whereas in the most extreme case an increase of 3 orders of magnitude in stability is observed. The green region corresponds to the single mutants where there are no H-bond donors on the porphyrin. The yellow region corresponds to the single mutants where the phosphonate groups have been removed from the ligand. The red region corresponds to the double mutants. The association constants are similar in the green and red regions, but there are some control complexes in the yellow region that show enhanced stability. Comparison between the complexes formed with ligands **L5b** and **L6b** and the complexes formed with ligands **L5c** and **L6c** suggests that it is interactions with

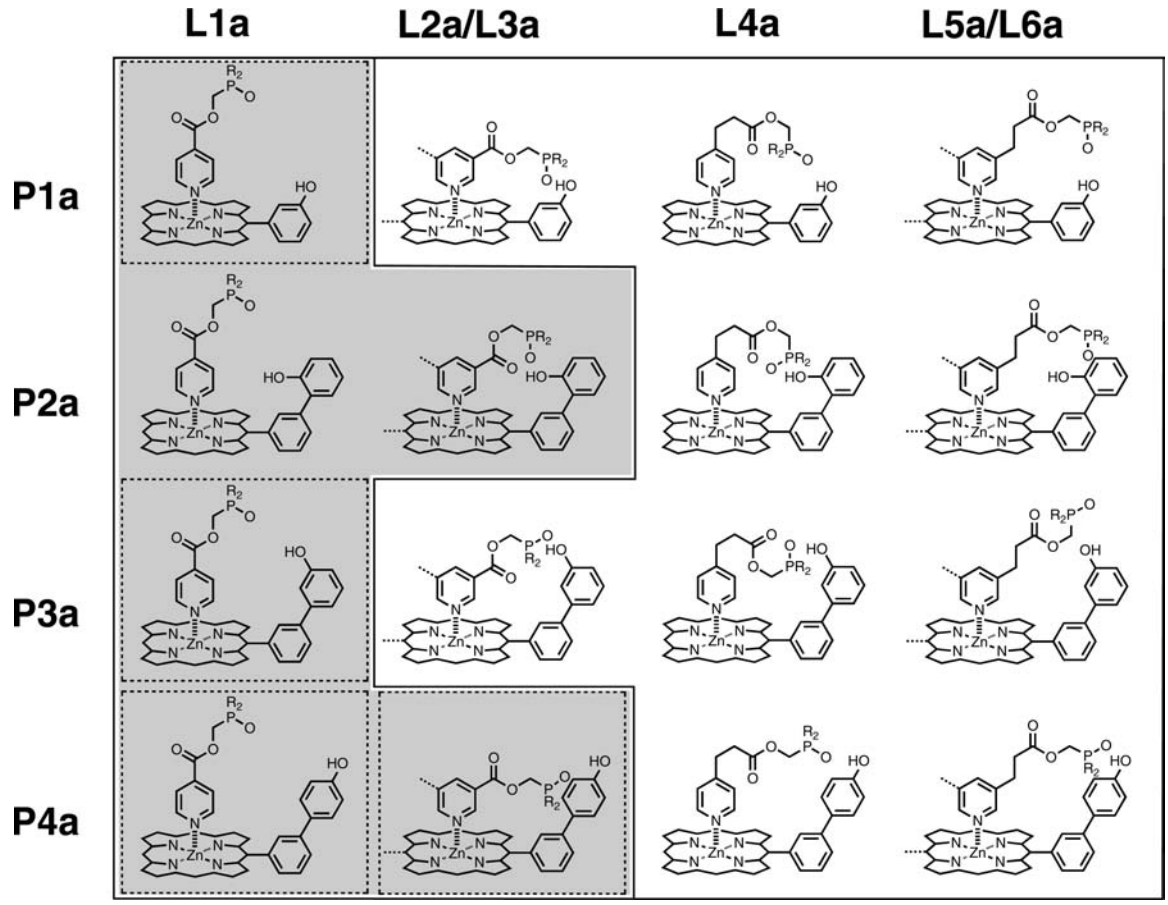

Figure 9. Illustration of possible geometries of different porphyrin−ligand combinations. The shaded areas correspond to systems where the contribution of a phosphonate diester−phenol H-bond to the overall stability of the complex is low ($\Delta\Delta G > -6$ kJ mol^{-1}): there are obvious geometric limitations on the formation of H-bonds in most of these systems. The four dotted boxes indicate systems that make 2:5 complexes. Ligands **L3a** and **L6a** have the same geometry as ligands **L2a** and **L4a**, respectively, but with a second side chain indicated by the dotted lines.

the ester carbonyl H-bond acceptors that are responsible for the enhanced stability of these yellow complexes. Thus, there is more than one kind of H-bond present, and the contributions of these multiple interactions have to be disentangled. The double mutant cycle approach is specifically designed to factor out the thermodynamic contributions of individual interactions. Figure 8 shows how the effects of ester−phenol H-bonding interactions can be removed to quantify the phosphonate−phenol H-bonds in complexes that make multiple H-bonds.

In complex A in Figure 8, there is the possibility of making both phosphonate diester−phenol and ester−phenol H-bonds. The overall stability of the complex reflects the contributions from metal−ligand binding, both types of H-bond, and any other secondary interactions that might be present. However, comparison of the stability of complex D with complex B provides a measure of the thermodynamic contribution of the ester−phenol H-bond. Comparison of complex D with complex C provides a measure of the contributions due to changes in the porphyrin−ligand coordination interaction. Thus, the DMC allows us to dissect the free energy contribution due to the phosphonate diester−phenol H-bond from all of the other interactions present in this system. This analysis assumes that all free energy contributions are additive. In other words, the presence of the phosphonate diester−phenol H-bond in complex A does not affect the stability of the ester−phenol H-bond as compared to the corresponding ester−phenol H-bond in complex B. This is an assumption that is difficult to verify experimentally, but there is experimental evidence that cooperative H-bond networks of this type behave in an additive manner with respect to free energy.[5c] Deviations from additivity are likely to be second-order effects as compared to the primary interactions, and if there are major secondary effects, they will show up as anomalies in the DMC analysis.

Table 2 summarizes the DMC results for all 24 complexes that can make phosphonate diester−phenol H-bonds. Ligands **L3a** and **L6a** both have two phosphonate diester groups and therefore have the potential to make two H-bonds, whereas the other ligands, **L1a**, **L2a**, **L4a**, and **L5a**, can only make one. Table 2 shows that the free energy contribution is approximately double for the ligands that have two H-bonding groups, **L3a** and **L6a**, when compared to the corresponding ligands that have one H-bonding group, **L2a** and **L5a**, respectively. This is rather good evidence for the additivity of the H-bond free energy contributions in these systems. There is considerable variation in the contributions due to H-bonding from one complex to another, and these differences can be rationalized to some extent on the basis of the geometries of the porphyrin−ligand combinations (Figure 9). For complexes where the phenol and phosphonate diester groups can achieve close proximity, there is a free energy contribution of -6 to -9 kJ mol^{-1} due to the formation of each H-bond. For the complexes where the H-bonding partners cannot get close to each other without major distortion, either in the metal−ligand geometry or in the configuration of the ester groups, the free energy contributions due to H-bonding are significantly weaker. It appears that for an optimal geometry the phosphonate diester−phenol H-bond

contributes −9 kJ mol^{-1}, and this is eroded by strain in the other complexes. There do not appear to be any significant contributions due to differences in conformational flexibility. Apart from the complexes that are highly strained, there is surprisingly little difference in the free energy contribution due to H-bonding from one architecture to another.

Thermodynamics of Ester−Phenol H-Bonding. As highlighted in Figure 7, there is evidence of increased stability in some of the control complexes due to the formation of ester−phenol H-bonds. By using a set of additional control ligands, **L4c**−**L6c**, it is possible to construct a different double mutant cycle to measure the thermodynamic contribution of these interactions to the overall stabilities of the complexes (Figure 10). In ligands **L1b**−**L3b**, the ester group is directly conjugated to the pyridine nitrogen, and so removal of the ester also has a significant effect on the metal−ligand interaction. However, this difference is accounted for in the double mutant cycle, because complexes A and C have the ester group and complexes B and D do not, so the change in the metal−ligand interaction cancels out.

Table 3 summarizes the results for all 24 complexes that can make ester−phenol H-bonds. It is clear that only ligands **L5b** and **L6b** make H-bonds. Moreover, in all cases, the free energy contributions due to H-bonding for ligand **L6b**, which has two ester groups, are approximately double that for ligand **L5b**, which has only one ester group. This again indicates that free energy increments due to H-bond interactions are additive in this system. The results can again be rationalized on the basis of the geometries of the complexes, as illustrated in Figure 11. For the systems that do not make H-bonds, the ester and phenol groups are too remote to interact without considerable strain. The exception is the **P2a·L2b/L3b** complex, which appears to be well-suited to the formation of H-bonds. However, the flat ChemDraw representation hides the fact that the dihedral angle around the biphenyl bond is closer to 90° than 0° in this system, due to the *ortho*-hydroxyl group. This appears to be sufficient to hold the two groups apart in this relatively rigid complex.

Each ester−phenol H-bond contributes a constant increment of −3 kJ mol^{-1} to the overall stability of the complex in these systems. This behavior is quite different from that observed for the phosphonate diester H-bonds. With the esters, it appears that H-bonding is an all or nothing process that depends on geometric complementarity. For the phosphonate diesters, the H-bonding interactions are significantly stronger, and so it is possible to trade off some of the binding energy in exchange for conformational strain to make more demanding contacts.

Structural Evidence for H-Bonding. The analysis above relies on the use of DMCs to determine thermodynamic contributions associated with particular functional group combinations. In essence, a more stable complex implies the presence of H-bond interactions. The implications of this analysis are that some of the complexes make as many as four H-bonds. For example, **P3a·L6a** is the most stable complex with an association constant of nearly 10^7 M^{-1}, and the DMC analysis indicates that both of the ester groups and both of the phosphonate diester groups make H-bonds with the porphyrin phenols. The schematic diagrams in Figures 9 and 11 show that this is geometrically feasible, and it is possible to construct full three-dimensional molecular models that confirm this (Figure 12).

To obtain direct experimental evidence for the presence of H-bonding interactions, we used ^{1}H NMR spectroscopy. The spectra were broad in deuterated toluene, but for some complexes, 1:1 mixtures of porphyrin and ligand gave well-resolved spectra in deuterated tetrachloroethane. The association constants are sufficiently high that the complexes are almost fully bound at a concentration of 1 mM. The phenol OH signals were generally shifted by +2−3 ppm relative to the corresponding signals in the spectra of the free porphyrin, indicative of the presence of H-bonding interactions. However, signal broadening and the sensivity of this signal to residual water precluded quantitative analysis.

The signals due to the porphyrin pyrrole protons proved more informative. Rotation around the porphyrin−*meso*-phenyl bond is slow on the ^{1}H NMR time scale at room temperature, leading to atropoisomers for all four receptors. For the free porphyrins, the presence of several atropisomers had no impact on the spectrum, and the pyrrole protons were observed as one singlet around 9 ppm (Figure 13a). Complexation of a simple ligand that does not form H-bonds led to a change of −0.1 ppm in the pyrrole signal, but did not affect the multiplicity (Figure 13b). Ligands that form one H-bond with one of the porphyrin *meso*-phenol substituents gave very similar spectra (Figure 13c). However, ligands that form more than one H-bond according to the DMC analysis above showed multiplicity in the pyrrole signal (Figure 13d−g). Ligands that make more than one H-bond have different affinities for different atropisomers, so they can be resolved in slow exchange in the NMR spectrum. Thus, complexes that form two H-bonds give the characteristic ^{1}H

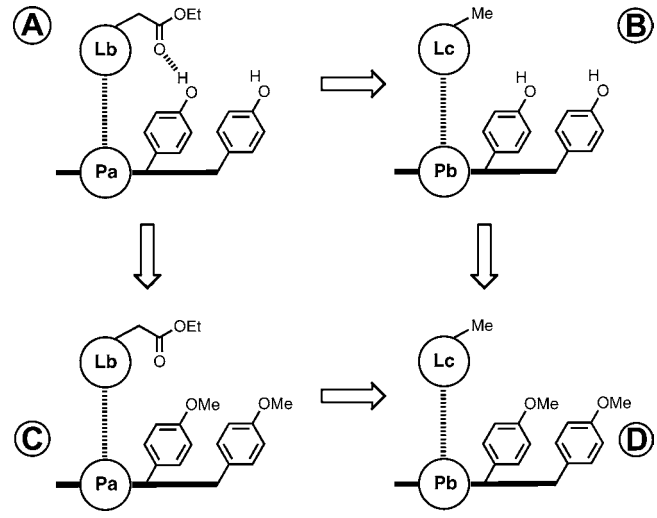

Figure 10. DMC for evaluating the thermodynamic contribution of ester−phenol H-bonds to the stability of a porphyrin−ligand complex.

Table 3. Free Energy Contributions from Ester−Phenol H-Bonds ($\Delta\Delta G°$/kJ mol^{-1}) at 298 K in Toluene, Determined Using the Chemical Double Mutant Cycle in Figure 10[a]

	ligand					
porphyrin	L1b	L2b	L3b	L4b	L5b	L6b
P1a	-1	0	0	0	-3	-5
P2a	0	0	0	0	-3	-6
P3a	0	-1	0	1	-3	-7
P4a	-1	-1	-1	0	0	0

[a] Complexes that do not make H-bonds are shaded (cf., Figure 11). Errors are ±1 kJ mol^{-1}.

(14) Barral, K.; Priet, S.; Sire, J.; Neyts, J.; Balzarini, J.; Canard, B.; Alvarez, K. *J. Med. Chem.* **2006**, *49*, 7799.

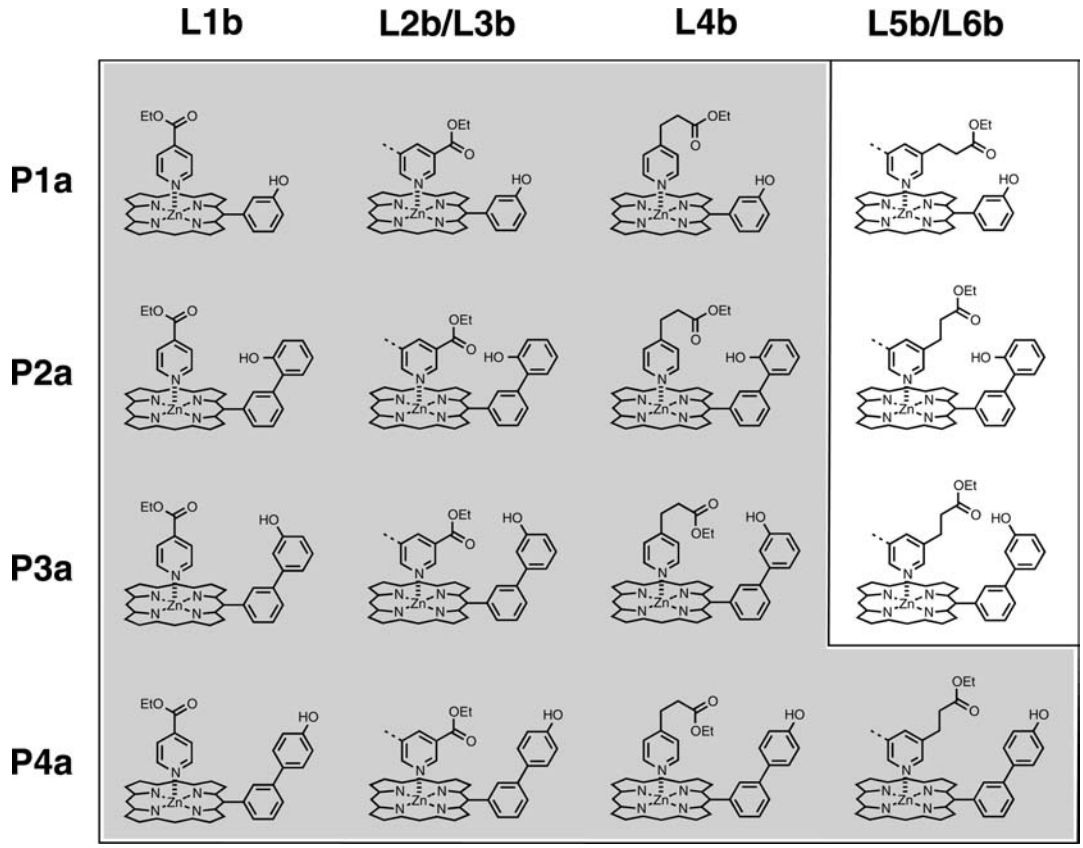

Figure 11. Illustration of possible geometries of different porphyrin−ligand combinations. The shaded areas correspond to systems that do not make ester−phenol H-bonds: there are obvious geometric limitations on the formation of H-bonds in most cases. Ligands **L3b** and **L6b** have the same geometry as ligands **L2b** and **L4b**, respectively, with a second side chain indicated by the dotted lines.

NMR spectra shown in Figure 13d and e. Complexes that form four H-bonds according to the DMC analysis also give rise to characteristic but different spectra (Figure 13f and g): the multiplicity in the pyrrole region is replaced by a single broad signal. In these cases, only one of the atropisomers can make four simultaneous H-bonds to the ligand, and so the atropisomer population is shifted to the symmetric α,α,α,α-isomer, resulting in a simpler spectrum. Although somewhat indirect, these observations corroborate the thermodynamic analysis from the DMCs above.

Partially Bound States. The DMC analysis allows us to separate the thermodynamic contributions from individual H-bond interactions to the overall stability of the complexes. These contributions are made up of two different components, the intrinsic strength of the H-bond interaction and the effective molarity (*EM*) for formation of the intramolecular contact. These two factors can be separated by comparing the intramolecular interactions, which we have measured above, with the corresponding intermolecular interactions between model compounds: phenol, **20**, phosphonate diester, **21**, and ester, **22** (Figure 14). The association constants for the **20·21** and **20·22** complexes were determined using ^{1}H NMR titrations in toluene, and the results are listed in Table 4. The value for the phenol−ester complex is at the limit of reliable experimental measurement, but the values of association constants for simple complexes of this type can also be estimated using eq 3.[7b] Table 4 shows that the experimental results are in good agreement with the values expected on the basis of H-bond parameters that have been determined independently for these functional groups.

$$-RT \ln K_{calc} = \Delta G^\circ = -(\alpha-\alpha_S)(\beta-\beta_S) + 6 \text{ kJ mol}^{-1} \quad (3)$$

Comparison of inter- and intramolecular H-bonding is complicated by the fact that the fully bound state may not be fully populated in systems that make multiple weak interactions. Figure 15 illustrates three different bound states that can be populated for ligands that make one coordination interaction and one H-bond. Because $K_0 \gg K_1$, state 1, where the porphyrin−ligand bond is broken, can be ignored, because it will not be significantly populated as compared to state 3, where the H-bond is broken. The population of partially bound state 3 depends on the product K_1EM. If $K_1EM \gg 1$, then the partially bound state will not be populated to any significant extent, and the overall stability of the complex will simply reflect the sum of the free energy contributions of the individual intermolecular contacts. However, if $K_1EM \approx 1$, then the fully and partially bound states (2 and 3 in Figure 15) will both be populated, and the thermodynamic properties of the complex will be a population weighted average of the properties of the different species (eq 4).

$$K_{obs} = K_0(1 + K_1EM) \quad (4)$$

For the porphyrin−ligand complexes that show phenol−ester H-bonding interactions, the increase in the stability of the complex is −3 kJ mol^{-1} per H-bond. A change in free energy of −3 kJ mol^{-1} corresponds to a value of K_1EM of 2 in eq 4, which means that the partially bound state is 30% populated, and we must therefore analyze the populations of states in more detail. As the number of different intermolecular interactions

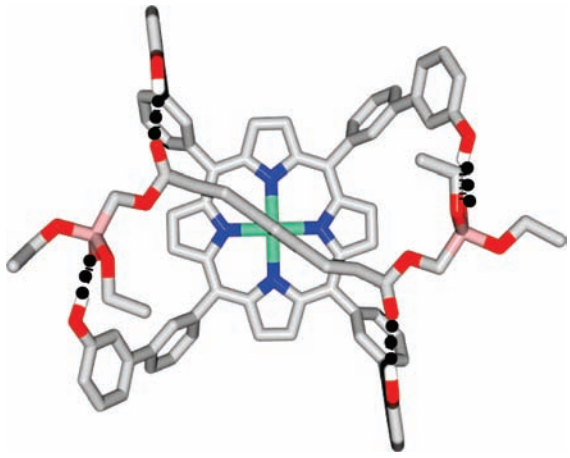

Figure 12. Three-dimensional structure of the **P3a·L6a** complex energy minimized using AM1.[17] There are four H-bonds (OH−O distances <2.2 Å) involving both of the ester groups and both of the phosphonate diester groups of the ligand.

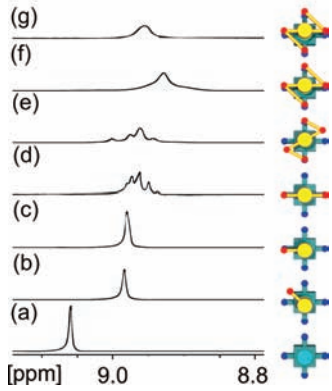

Figure 13. Pyrrole region of the ^{1}H NMR spectra of (a) [**P3a**] = 1 mM with no ligand, (b) [**P3a**] = [**L4b**] = 1 mM (no H-bonds), (c) [**P3a**] = [**L5b**] = 1 mM (one H-bond), (d) [**P3a**] = [**L6b**] = 1 mM (two H-bonds), (e) [**P4a**] = [**L6a**] = 1 mM (two H-bonds), (f) [**P1a**] = [**L6a**] = 1 mM (four H-bonds), and (g) [**P3a**] = [**L6a**] = 1 mM (four H-bonds) in deuterated tetrachloroethane.

increases in the more complex systems, the number of partially bound states that are possible increases, and this affects any attempt to deconvolute the thermodynamic contributions of individual interaction sites.

In general, for complexes that make N intramolecular H-bonds, the observed association constant is given by the sum of the equilibrium constants for all of the bound states (eq 5).

$$K_{obs} = K_0(1 + \sum_i \sigma_i K_i EM_i + \sum_{i,j}^{N} \sigma_{ij} K_i EM_i K_j EM_j + ... + \sigma_{ij...N} \prod_i^N K_i EM_i) \quad (5)$$

where K_0 is the intermolecular association constant for formation of the zinc−nitrogen interaction, K_i is the intermolecular association constant for formation of the relevant H-bonding interaction, EM_i is the effective molarity for formation of the intramolecular interaction, and σ_i is the statistical factor that describes the degeneracy of the partially bound state.[15]

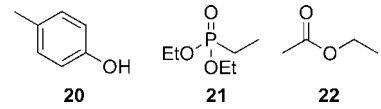

20 **21** **22**

Figure 14. Model compounds used to quantify intermolecular H-bond interactions.

Table 4. Association Constants (M^{-1}) for the Formation of H-Bonded Complexes in Toluene-d_8 at 298 K Measured by ^{1}H NMR Titrations (K_{expt}) and Estimated Using Eq 3 (K_{calc})[a]

complex	α	β	α_S	β_S	K_{expt}	K_{calc}
20·21	3.8	8.9	1.0	2.2	140 ± 10	180
20·22	3.8	5.3	1.0	2.2	3 ± 1	3

[a] H-bond parameters, α and β, from ref 9.

The population of the fully bound state, P_b, is given by eq 6.

$$P_b = \frac{K_0 \sigma_{ij...N} \prod_i^N K_i EM_i}{K_{obs}} \quad (6)$$

The populations of the partially bound states, where only some of the intramolecular H-bond are made, can be determined in a similar way.

The approach is illustrated below for complexes that can make a single intramolecular H-bond, and full details for the more complex systems can be found in the Supporting Information. For a single intramolecular H-bond, the observed association constant is given by the sum of the equilibrium constants for the fully bound and one partially bound state (eq 7).

$$K_{obs} = K_0(1 + \sigma_1 K_1 EM_1) \quad (7)$$

where K_0 is the intermolecular association constant for formation of the zinc−nitrogen interaction, K_1 is the intermolecular association constant for formation of the H-bonding interaction, EM_1 is the effective molarity for the intramolecular interaction, and σ_1 is the statistical factor that describes the degeneracy of the fully bound state. In the complexes discussed here, the porphyrins all have four identical H-bond donor sites, so $\sigma_1 = 4$.

The population of the fully bound state, P_b, is given by

$$P_b = \frac{\sigma_1 K_1 EM_1}{1 + \sigma_1 K_1 EM_1} \quad (8)$$

and the population of the partially bound state, P_f, where the intramolecular H-bond is not made is given by

$$P_f = \frac{1}{1 + \sigma_1 K_1 EM_1} \quad (9)$$

Note that the key parameter that defines the behavior of the system is the product $\sigma_1 K_1 EM_1$. When $\sigma_1 K_1 EM_1 \ll 1$, the H-bonded state is not populated. In the limit of $\sigma_1 K_1 EM_1 \gg 1$, the partially bound state is not populated, and eq 7 reduces to $K_{obs} = \sigma_1 K_0 K_1 EM_1$, which is the basis for the double mutant cycle analysis above. In general, the value of $\Delta\Delta G^0$ obtained from the DMC provides a measure of the ratio K_{obs}/K_0 corrected for any secondary interactions and substituent effects and so can be used to determine effective molarities (eq 10).

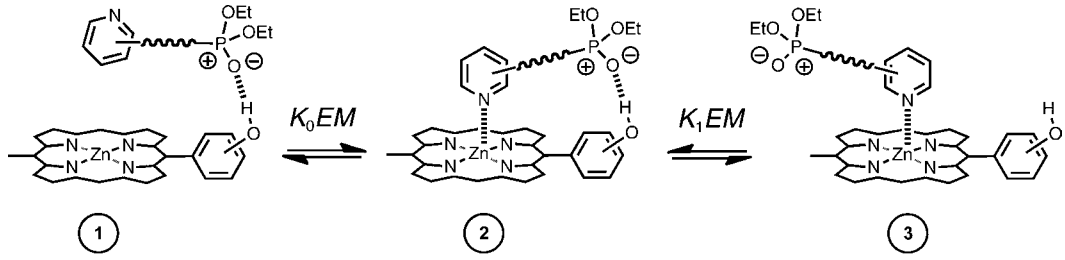

Figure 15. Different bound states that are possible in a 1:1 complex between a porphyrin and a ligand that can make one H-bond and one coordination interaction. K_0 is the intermolecular association constant for porphyrin−ligand coordination. K_1 is the intermolecular association constant for the H-bonded complex. *EM* is the effective molarity for the intramolecular interaction.

$$e^{-\Delta\Delta G^{\circ}/RT} = \frac{K_{obs}}{K_0} = 1 + \sigma_1 K_1 EM_1 \qquad (10)$$

Effective Molarities. The DMC free energies in Tables 2 and 3 were used in conjunction with the intermolecular association constants in Table 4 and the partially bound states analysis in the Supporting Information to determine effective molarities for the intramolecular H-bonds observed in these systems. The results are summarized in Tables 5 and 6. The variations in the values of *EM* with both ligand and receptor structure are surprisingly small. In most cases, the intramolecular phosphonate diester−phenol H-bonds have an *EM* of about 30 mM. In cases where the geometry is particularly unfavorable, this values drops by an order of magnitude, and in two cases, H-bonding cannot be detected (shaded boxes in Table 5). Neither differences in ligand side chain flexibility nor the formation of additional H-bonds with the ester linkers, which might be expected to organize the ligand side-chains, seem to have a major effect on *EM* in these systems.

The *EM* is an order of magnitude higher for the intramolecular ester−phenol H-bonds, 200 mM. The ester and phosphonate diester H-bond groups are located at different positions on the ligand framework, which means that the *EM* values cannot be directly compared. However, we have explored a large number of different geometries, so the results suggest that there is an intrinsic difference in the ability of these two functional groups to form intramolecular interactions. One possibility is that the increased steric crowding around the phosphonate group interferes with the formation of strong intramolecular interactions.

In general, the values of σKEM for intramolecular phosphonate diester H-bonds are around 10, which means that these interactions are 90% bound, and partially bound states do not play a significant role. The value of σKEM drops in the more strained complexes highlighted by the shaded boxes in Table 5, so partially bound states are populated. These are the cases in which the formation of the higher order 2:5 complexes complicates analysis of the titration data. For intramolecular ester−phenol H-bonds, the value of σKEM is around 2, so these interactions are never more than 60% populated.

Conclusions

The metalloporphyrin−ligand architecture provides an ideal platform for conducting a systematic survey of the relationship between chemical structure and cooperativity at relatively complex molecular recognition interfaces. In this Article, we have developed an approach to dissecting cooperative networks of noncovalent interactions based on chemical double mutant cycles. Systematic deletion of functional groups allows quantification of the free energy contributions of individual functional group contacts, and these have been characterized in terms of effective molarities for the intramolecular processes. Exploitation of an automated UV/vis titration system has enabled straightforward characterization of 120 different porphyrin−ligand combinations, and these data have been used to construct a large of number of different DMCs to examine a variety of closely related intramolecular H-bonds in different supramolecular architectures. The number of intramolecular H-bonds formed varies from zero to four depending on geometric complementarity and the number of functional groups on the ligand, but, in all cases, the free energy contribution from each functional group contact could be dissected using appropriate DMCs.

Two types of H-bond were detected: between phosphonate diester H-bond acceptors on the ligand and phenol H-bond donors on the porphyrin, and between carboxylate ester acceptors on the ligand and phenol donors on the porphyrin. As expected from the properties of simple intermolecular H-bonds measured for model compounds, the intramolecular phosphonate diester H-bonds contribute significantly more to the stability of the complexes (−6 to −9 kJ mol^{-1}) than do the carboxylate ester H-bonds (−3 kJ mol^{-1}). However, the two classes of interaction show qualitatively very different behavior. The weak carboxylate ester H-bonds show all-or-nothing behavior: when there is good geometric complementarity between the ligand and receptor, a H-bond is observed, and when there is not, there

Table 5. Effective Molarities (*EM*/mM) for Intramolecular Phosphonate Diester−Phenol H-Bonds Measured at 298 K in Toluene[a]

	ligand					
porphyrin	L1a	L2a	L3a	L4a	L5a	L6a
P1a	*b*	45	63	38	45	48
P2a	10	*b*	7	15	24	37
P3a	5	25	17	64	28	25
P4a	5	7	4	43	24	26

[a] Complexes that make weak or no H-bonds are shaded (cf., Figure 9). Errors are ±40%. [b] No interaction detected.

Table 6. Effective Molarities (*EM*/mM) for Intramolecular Ester−Phenol H-Bonds Measured at 298 K in Toluene[a]

	ligand					
porphyrin	L1b	L2b	L3b	L4b	L5b	L6b
P1a	*b*	*b*	*b*	*b*	180	160
P2a	*b*	*b*	*b*	*b*	220	220
P3a	*b*	*b*	*b*	*b*	180	280
P4a	*b*	*b*	*b*	*b*	*b*	*b*

[a] Complexes that do not make H-bonds are shaded (cf., Figure 11). Errors are ±50%. [b] No interaction detected.

is no H-bond. The stronger phosphonate diester H-bonds make intramolecular contacts even in cases where there is a significant geometrical mismatch between the ligand and the receptor. In these cases, the associated strain leads to a decrease in the free energy contribution to the overall stability of the complex as compared to the −6 to −9 kJ mol^{-1} observed for the more complementary architectures. Thus, H-bonds to phosphonate diesters were observed for 22 of the 24 systems examined, whereas H-bonds to carboxylate esters were observed in only 6 of the 24 geometries studied.

The magnitude of the cooperativity involved in the formation of the intramolecular interactions was quantified using the effective molarity (*EM*). There is remarkably little variation in the value of *EM* with supramolecular architecture, conformational flexibility, geometric complementarity, and number of interactions. In the phosphonate diester series, the *EM* is around 30 mM for 16 of the 24 systems studied, but it drops to 5 mM when there is significant geometric strain. In the carboxylate ester series, the *EM* is around 200 mM in all 6 systems that make intramolecular H-bonds. The large difference between the two sets of *EM* values is striking, given that both series cover a range of different architectures. There are two possible explanations: the phosphonate diester groups are very bulky and steric constraints may prevent them from reaching optimal geometries in the confined spaces on the faces of the receptors; or there may be some kind of compensation effect, where the stronger H-bond constrains the interacting groups more tightly leading to a lower *EM*. Extending this survey to a wider range of functional groups would provide further insight into the origin of this effect.

The analysis in this Article is based on the assumption that free energy contributions from different functional group interactions are additive, and the self-consistency of the results obtained supports this assumption. For example, the free energy contribution due to H-bonding in ligands that have two symmetrical side arms is almost exactly double that for the corresponding ligands, which have only one side arm in all cases. This suggests that simple additive schemes, such as the Free−Wilson analysis,[16] have some validity even in complex systems where multiple cooperative interactions are present.

Experimental Section

Automated UV/Visible Absorption Titrations. UV/vis titrations were carried out by preparing a 10 mL sample of porphyrin at known concentration (3−7 μM) in spectroscopic grade solvent. A 10 mL solution of ligand (40−5000 μM) was prepared using spectroscopic grade solvent (i.e., without any host present). 150 μL of porphyrin solution was added to each well of a 96 well Hellma quartz plate, and the UV/vis absorbance was recorded at five wavelengths using a BMG FLUOstar Omega plate reader. The plate reader was thermostatted at 298 K for all measurements. Aliquots of ligand solution (3, 6, or 10 μL) were added successively to each well containing the porphyrin solution, and the UV/vis absorbance was recorded after each addition. Changes in the absorbance of the Soret band of the porphyrin were fit to a 1:1 binding isotherm in Microsoft Excel to obtain the association constant. Each titration was repeated at least three times, and the experimental error is quoted as twice the standard deviation at a precision of one significant figure.

Manual UV/Visible Absorption Titrations. UV/vis titrations were carried out by preparing a 10 mL sample of porphyrin at known concentration (0.5−7 μM) in spectroscopic grade solvent. Two milliliters of this solution was removed, and a UV/vis spectrum was recorded using a Peltier thermostat set at 298 K. A 2 mL solution of ligand (40−3000 μM) was prepared using the porphyrin stock solution, so that the concentration of porphyrin remained constant throughout the titration. Aliquots of ligand solution were added successively to the cell containing the porphyrin solution, and the UV/vis spectrum was recorded after each addition. Changes in the absorbance of the Soret band of the porphyrin were fit to a 1:1 binding isotherm in Microsoft Excel to obtain the association constant. Each titration was repeated at least three times, and the experimental error is quoted as twice the standard deviation at a precision of one significant figure.

^{1}H NMR Titrations. NMR titrations were carried out by preparing a 2 mL sample of host at known concentration (7−270 mM). Next, 0.6 mL of this solution was removed, and a ^{1}H NMR spectrum was recorded. A 1 mL solution of guest (70−2600 mM) was prepared using the host solution, so that the concentration of host remained constant throughout the titration. Aliquots of guest solution were added successively to the NMR tube containing the host, and the NMR spectrum was recorded after each addition. Changes in chemical shifts were analyzed by using the appropriate binding isotherms in Microsoft Excel. Each titration was repeated at least three times, and the experimental error is quoted as twice the standard deviation at a precision of one significant figure.

Acknowledgment. We thank the EPSRC for funding and Dr. M. Fisher for assistance with protocols for the BMG Labtech plate reader.

Supporting Information Available: Synthetic procedures and spectroscopic data, protocol for operation of the UV/vis plate reader, details of the fitting of the titration data to different binding isotherms, analysis of partially bound states for systems that make more than one H-bond, and tables of *K EM* values and occupancies for intramolecular H-bonds and coordinates of the structure shown in Figure 12. This material is available free of charge via the Internet at http://pubs.acs.org.

JA1084783

(15) (a) Bailey, W. F.; Monahan, A. S. *J. Chem. Educ.* **1978**, *55*, 489–493. (b) Ercolani, G.; Piguet, C.; Borkovec, M.; Hamacek, J. *J. Phys. Chem. B* **2007**, *111*, 12195–12203.

(16) (a) Free, S. M.; Wilson, J. W. *J. Med. Chem.* **1964**, *7*, 395. (b) Andrews, P. R.; Craik, D. J.; Martin, J. L. *J. Med. Chem.* **1984**, *27*, 1648–1657. (c) Tomic, S.; Nilsson, L.; Wade, R. C. *J. Med. Chem.* **2000**, *43*, 1780–1792. (d) Gohlke, H.; Klebe, G. *Angew. Chem., Int. Ed.* **2002**, *41*, 2645–2676.

(17) (a) Conformations were analyzed using an MMFFs MCMM search using Macomodel, and the lowest energy conformation was minimized at a semi-empirical AM1 level using Spartan 06. (b) *Macromodel (Version 7.1)*; Schrödinger, Inc.: Portland, OR, 2000, running on a Linux cluster. (c) *Spartan 06*; Wavefunction, Inc.: Irvine, CA, running on a Windows PC.